ResearchGate

See discussions, stats, and author profiles for this publication at: https://www.researchgate.net/publication/224861275

Electrochemical Impedance Study of the Hematite/Water Interface

ARTICLE *in* LANGMUIR · APRIL 2012

Impact Factor: 4.46 · DOI: 10.1021/la300829c · Source: PubMed

CITATIONS
24

READS
129

3 AUTHORS:

Kenichi Shimizu
University of Oxford
17 PUBLICATIONS **311** CITATIONS
SEE PROFILE

Andrzej Lasia
Université de Sherbrooke
150 PUBLICATIONS **3,996** CITATIONS
SEE PROFILE

Jean-Françoi Boily
Umeå University
87 PUBLICATIONS **1,648** CITATIONS
SEE PROFILE

Available from: Kenichi Shimizu
Retrieved on: 02 February 2016

Langmuir

Article

pubs.acs.org/Langmuir

Electrochemical Impedance Study of the Hematite/Water Interface

Kenichi Shimizu,[†] Andrzej Lasia,[‡] and Jean-François Boily*,[†]

[†]Department of Chemistry, Umeå University, Umeå SE-901 87, Sweden

[‡]Department of Chemistry, University of Sherbrooke, Sherbrooke QC J1K 2R1, Canada

ABSTRACT: Reactions taking place on hematite (α-Fe_2O_3) surfaces in contact with aqueous solutions are of paramount importance to environmental and technological processes. The electrochemical properties of the hematite/water interface are central to these processes and can be probed by open circuit potentials and cyclic voltammetric measurements of semiconducting electrodes. In this study, electrochemical impedance spectroscopy (EIS) was used to extract resistive and capacitive attributes of this interface on millimeter-sized single-body hematite electrodes. This was carried out by developing equivalent circuit models for impedance data collected on a semiconducting hematite specimen equilibrated in solutions of 0.1 M NaCl and NH_4Cl at various pH values. These efforts produced distinct sets of capacitance values for the diffuse and compact layers of the interface. Diffuse layer capacitances shift in the pH 3−11 range from 2.32 to 2.50 $\mu F \cdot cm^{-2}$ in NaCl and from 1.43 to 1.99 $\mu F \cdot cm^{-2}$ in NH_4Cl. Furthermore, these values reach a minimum capacitance at pH 9, near a probable point of zero charge for an undefined hematite surface exposing a variety of (hydr)oxo functional groups. Compact layer capacitances pertain to the transfer of ions (charge carriers) from the diffuse layer to surface hydroxyls and are independent of pH in NaCl, with values of 32.57 ± 0.49 $\mu F \cdot cm^{-2} \cdot s^{-\varphi}$. However, they decrease with pH in NH_4Cl from 33.77 at pH 3.5 to 21.02 $\mu F \cdot cm^{-2} \cdot s^{-\varphi}$ at pH 10.6 because of the interactions of ammonium species with surface (hydr)oxo groups. Values of φ (0.71−0.73 in NaCl and 0.56−0.67 in NH_4Cl) denote the nonideal behavior of this capacitor, which is treated here as a constant phase element. Because electrode-based techniques are generally not applicable to the commonly insulating metal (oxyhydr)oxides found in the environment, this study presents opportunities for exploring mineral/water interface chemistry by EIS studies of single-body hematite specimens.

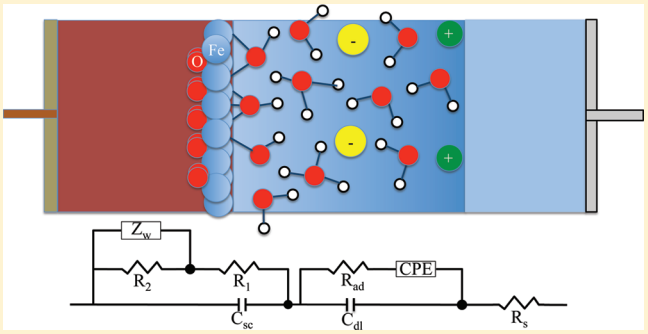

1. INTRODUCTION

Processes occurring at hematite/water interfaces play critical roles in a variety of natural and technological processes. Hematite is an abundant mineral in the earth's crust and contributes to several biogeochemical cycles.[1] It also has various industrial applications, given its high chemical robustness, mechanical strength, facile synthesis, attractive band gap (2.1 eV), and low cost. For instance, it is considered for photoassisted water-splitting reactions and in the fabrication of gas-sensing electrodes.[2] A fundamental knowledge of the properties controlling the hematite/water interface reactivity is thereby important to predicting the behavior of this important mineral in these different settings.

Fundamental experimental studies on hematite/water interface chemistry have focused on various forms of colloidal particles[3−7] as well as single or cut crystals.[8−18] Recent notable efforts along these fronts led to interfacial water structures,[9−13] ion adsorption,[14−16] and electric potentials[19−24] of this important system. Although interfacial electrical potentials, other than shear plane potentials, are generally not measurable in insulating metal (oxy)(hydr)oxides of environmental interest, some hematite specimens can be found or made with sufficient *n*-type semiconductivity to be used as electrode materials. Hematite electrode surfaces have consequently been used to follow interfacial reactions, including potential following, ion adsorption,[19,21] ligand-promoted etching,[21] surface-to-bulk electron transfer,[20] and photoassisted water splitting.[6,7] Open circuit potentials and cyclic voltammetry are common measurement approaches in these cases. Electrochemical impedance spectroscopy (EIS) has received, in contrast, much less attention in the study of hematite,[25−28] although it is a very sensitive technique for studying interfacial phenomena, including fundamental reaction kinetics and mechanisms.[29−31]

EIS measures the opposition of flow of an alternating current of various frequencies applied to a cell, such as a hematite body in contact with an aqueous solution (Figure 1). The ratio of Fourier transforms of voltage and current can then be modeled using an equivalent circuit consisting of a combination of resistors and capacitors representing various frequency-resolved interfacial processes (Figure 1). These measurements can notably be used to distinguish between slow chemical reactions and fast electrostatic reactions involving the transfer of ions through compact and diffuse layers. The few EIS studies of

Received: February 27, 2012
Revised: April 19, 2012
Published: April 27, 2012

 © 2012 American Chemical Society

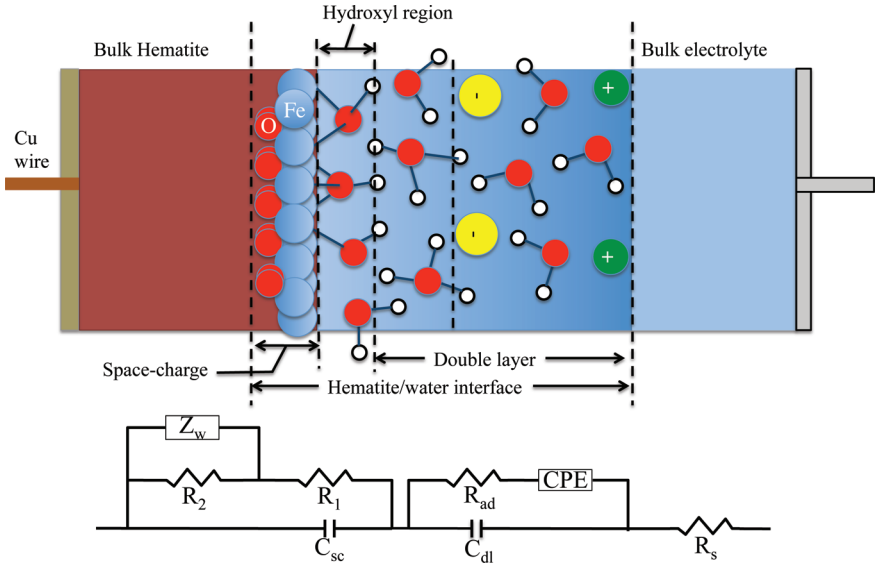

Figure 1. Schematic view of the hematite/water interface in the electrode setup (top) and the equivalent circuit model used for EIS modeling (bottom). The equivalent circuit model consists of two components: the solid phase and the aqueous phase. The solution side of the interface is represented by the following circuit components: solution resistance (R_s), a diffuse layer capacitance (C_{dl}), and a CPE as well as a resistance (R_{ad}) for charge-carrier transfer from the diffuse to the compact layer. The solid-phase terms include the capacitance of the space charging layer (C_{sc}), the ohmic resistance (R_1), and the charge transport (R_2) and charge diffusion (Z_w).

hematite have so far involved nanosized materials either deposited on or oxidized from a conductive electrode surface.[6,25−28] In both cases, however, undesirable contributions from the electrode matrix can pose serious challenges to interpretations of impedance data when the interest lies solely in processes taking place on hematite, such as in our case. Measurements of a single surface should, in this respect, be highly desirable for more straightforward interpretations of EIS data and toward the elucidation of key processes and the extraction of electrical double layer parameters of the hematite/water interface.

In this study, we present, to the best of our knowledge, the results of the first EIS measurements of a single-body hematite electrode. The approach adopted in this work uses tightly controlled experimental conditions to investigate systematic effects of variations of pH on the EIS data of a hematite electrode in contact with aqueous solutions of NaCl and NH_4Cl. The interest in these conditions lies in our previous efforts whereby cryogenic X-ray photoelectron spectroscopy (XPS) was used to track electrolyte cation loadings on nanosized hematite particles.[3,5,32] Furthermore, the ability of the ammonium ion to form a hydrogen bond with surface hydroxo groups is of general importance in biogeochemical, atmospheric, and technological settings. This study seeks to build upon our recent results by extracting resistive and capacitive attributes of the hematite/water interface under these conditions. Although this study makes use of an electrode with a relatively unconstrained surface orientation, in an effort to emulate undefined surfaces in our previously studied nanosized particles,[3,5,32] a follow-up study on surfaces with known and controlled crystallographic orientations will shortly appear. This current study demonstrates the overall feasibility of EIS methods in the study of macrosized single-body hematite electrodes, details an equivalent circuit that can be used in further studies of the hematite/water interface, and provides experimentally derived interfacial properties.

2. EXPERIMENTAL SECTION

A 4.99 mm × 4.44 mm × 2.05 mm natural hematite specimen from an unspecified location in Brazil was obtained from SurfaceNet (Rheine, Germany). It was originally cut, chemically and mechanically polished along the (001) plane, and then sonicated in acetone. The specimen was thereafter annealed at 1000 °C for 17 h in air, mechanically repolished with pads of various mesh sizes, hand polished to a mirror finish using an aqueous slurry of 5 μm alumina, and then finally sonicated in Millipore water to remove any polishing residues. It is therefore important to note that the resulting surface is not the pristine (001) plane and may be populated by a variety of surface (hydr)oxo groups; the results for pristine surfaces will be reported shortly. X-ray photoelectron spectroscopy (Kraton Axis Ultra) retrieved the characteristic Fe $2p_{3/2}$ and O 1s lines of hematite and 7.20% impurities (1.12% F, 1.90% Cr, 0.07% Ag, 0.18% Ca, 1.64% Mo, 2.28% Si, and 0.01% Pb).

The hematite working electrode was fixed in a Tygon tube using epoxy resin and electrically connected to a Cu wire using Ag epoxy, exposing only its 4.99 mm × 4.44 mm polished surface. The electrode was dried at 80 °C for 20 min, rinsed in acetone, and dried under N_2(g) at room temperature. It was then encased in a sealed titration vessel for electrochemical measurements. These measurements were carried out using the conventional three-electrode cell configuration consisting of the working hematite electrode, an Ag/AgCl reference electrode (3 M KCl, BASi), and a platinum mesh auxiliary electrode. Alkalimetric titration experiments were conducted in 0.1 M NH_4Cl and NaCl solutions under an atmosphere of N_2(g). Experiments were started at pH 3 to 4 under conditions where the solutions were degassed from dissolved CO_2(g). The pH was thereafter adjusted with standard NH_4OH or NaOH prepared at the same ionic strength and ionic composition as the background electrolyte. The cell's open circuit potential (E_{ocp}) was measured for at least 40 min at each pH value under mechanical stirring. Its final value was recorded once a drift of less than 0.3 mV/min was achieved. This was typically reached within 50 min. An EIS measurement was thereafter carried out at this potential, after which the titration was continued.

EIS measurements of the electrode exposed to aqueous solutions were carried out at bias potentials equal to E_{ocp} during which the frequency was changed from 100 kHz to 0.1 Hz with a working amplitude of 25 mV. The impedance data was validated using the Kramers−Kronig transform test[33,34] and then fitted to the equivalent

dx.doi.org/10.1021/la300829c | Langmuir 2012, 28, 7914−7920

circuit model of Figure 1 using the program ZView (v. 3.1). A variety of models were tested during the course of these procedures. The circuit of Figure 1 was chosen on the basis of its ability to reproduce the data, using statistical analyses to determine the optimal number of significant adjustable parameters objectively.

Electrochemical analyses were conducted using a Princeton Applied Research 273A potentiostat/galvanostat with a model 1250A frequency response analyzer (Solartron Analytical). This instrument was also used to test the current response of the electrode in a separate set of experiments by cyclic voltammetry. Finally, the intrinsic resistivity (10.9 kΩ) of the hematite single body was independently measured by EIS by electrically connecting the upper and lower 4.99 mm × 4.44 mm surfaces of the electrode to a Cu wire using Ag epoxy.

3. RESULTS AND DISCUSSION

3.1. Electrode Current Response. Cyclic voltammetry confirmed the functionality of the electrode (Figure 2), with

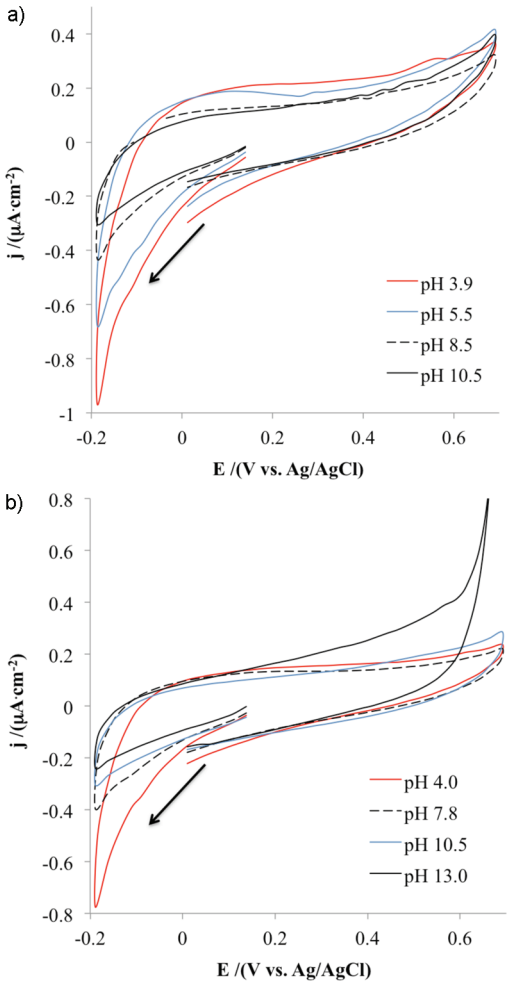

Figure 2. Cyclic voltammograms of a single-body hematite electrode in (a) 0.1 M NH_4Cl and (b) 0.1 M NaCl. Data was collected under a $N_2(g)$ atmosphere at a sweep rate of 5 mV s^{-1}.

voltammograms showing increasing current density toward the cathode. Larger currents that developed at low pH are attributed to the reductive dissolution of the hematite surface, as shown by Mulvaney et al.[35] and Jang et al.[36] Changes in the anodic current response with pH are not as clear as for the cathodic current response, save the sharp rise in the NaCl-bearing solution at pH 13 (Figure 2b). Comparable anodic responses under such alkaline conditions were reported by Cummings et al.[37] and Bora et al.[38] and may result from Fe^{III} oxidation to Fe^{IV}.[39−41] This issue remains, at any rate, outside the main scope of the current work, yet further investigation along this front is clearly needed.

Cyclic voltammetry can also ideally be used to determine the entire interfacial capacitance (C_{int}) of the system, here defined as the entire region encompassing both compact and diffuse layers (Figure 1). These values can be obtained from the steady-state current (j) and the sweep rate (υ) according to the relation $j = \upsilon C_{int}$.[42] Although these results (Figure 3) were

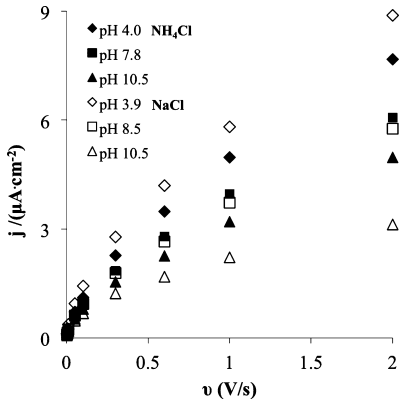

Figure 3. Steady-state current (j) as a function of the sweep rate (υ) obtained by cyclic voltammetry.

nonlinear over the entire range of considered scan rates (0.002−2 V·s^{-1}) possibly because of charge transfer in the space charge region (depletion layer), the nearly linear dependence of the 0.3−2 V·s^{-1} range can be used to extract approximate values. C_{int} values obtained by this approach decrease with pH and from 3.1 to 2.0 μF·cm^{-2} in NaCl and from 3.5 to 1.1 μF·cm^{-2} in NH_4Cl. The 1.1 μF·cm^{-2} value appears only at pH 10.5 and arises from specific interactions between ammonia and surface hydroxyl groups, as will be emphasized later through the more complete analyses of the EIS data.

3.2. Electrode Potential Development. E_{OCP} values (Figure 4) were collected prior to each EIS measurements.

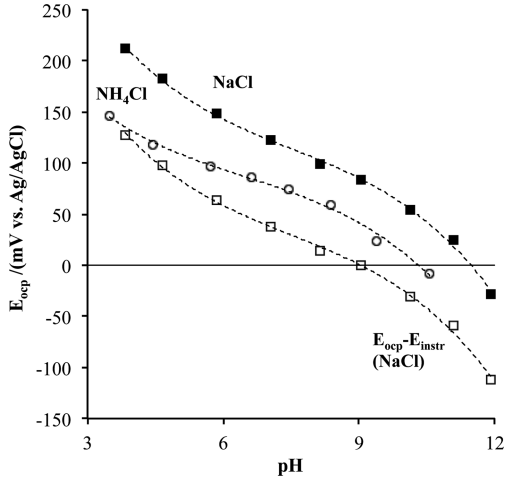

Figure 4. Open circuit potential (OCP) of the hematite electrode in 0.1 M NaCl and NH_4Cl. The $E_{ocp}-E_{inst}$ curve shows the offset of NaCl E_{ocp} data such that E_{ocp} = 0 at PZC = 9.

dx.doi.org/10.1021/la300829c | Langmuir 2012, 28, 7914−7920

These values exhibit sub-Nernstian values of about −27 mV/pH in NaCl and −20 mV/pH in NH_4Cl. Because our electrode is not terminated by the pristine (001) plane, various surface groups ($\equiv Fe_xOH$, where x = 1, 2, 3) contribute to potential development on this surface. The elucidation of these specific effects will be reported in a forthcoming study using electrodes with well-defined crystallographic orientations. Our results nonetheless remain in qualitative agreement with titrations of the (001) surface by Zarzycki et al.[19] but not those of Boily et al.,[21] which were obtained using more stringent equilibration criteria. The Zarzycki et al.[19] data were deliberately obtained by a rapid set of titrations exhibiting strong hysteresis whereby equilibrium values were predicted using a Maxwell construction approach. In the course of preliminary sets of experiments, we also performed such rapid titrations. An examination of time-resolved E_{ocp} values confirmed that deprotonation/discharging reactions were sluggish in comparison to protonation/charging reactions. An analysis of these data, using the same methodology as in Zarzycki et al.,[19] yields comparable, although not identical, values to our E_{ocp}. Therefore, although a truly equilibrated system would require waiting periods of several hours, our E_{ocp} data can be considered to arise from steady-state-like conditions for the duration (~8 min) of the EIS measurements, as well as in relation to our working amplitude of 25 mV.

3.3. EIS of the Hematite/Water Interface. *3.3.1. Equivalent Circuit Model.* In contrast to the cyclic voltammetry efforts, EIS enables the extraction of capacitance values for various components of an equivalent circuit representing the frequency-dependent impedance data. Impedance (Z) values of the various components are added in series or in parallel according to the circuit's configuration. Impedance data were collected with the bias potential set to the aforementioned steady-state E_{OCP} (Figure 4). Note that Faradaic processes do not pertain under those conditions, as shown by cyclic voltammetry (Figure 2). Characteristic impedance spectra of hematite in NaCl and NH_4Cl solutions are presented in Figure 5 as complex plane plots. All impedance curves take the form of distorted semicircles in the high-frequency region, whereas the intermediate- and low-frequency regions adopt a nearly linear increase in impedance. Overall, the impedance response of our system is determined by (i) the hematite bulk, (ii) the interfacial region comprising a compact layer and a diffuse layer, (iii) the bulk electrolyte region, and (iv) other instrument components (Figure 1).

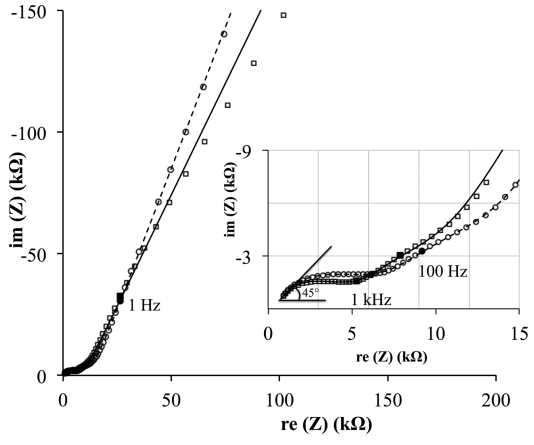

Figure 5. Representative complex plane plots (re = real; im = imaginary) for the hematite electrode in (○) NaCl at pH 3.8 and (□) NH_4Cl at pH 3.5. (Inset) Complex plane plots for the high-frequency region. Full and dashed lines show fits obtained with the equivalent circuit model of Figure 1, using eqs 1 and 2, respectively. Modeling parameters are reported in Table 1. Landmark frequencies are also indicated.

A variant of the circuit model of Bondarenko and Ragoisha,[43] originally developed on a TiO_2 single-body electrode, was adopted to model our impedance data. Our proposed circuit, developed to provide statistically good fits to all EIS data, can be broken down into bulk hematite, hematite/water interface, and solution components.

Contributions from the hematite bulk include (i) ohmic resistance ($Z_1 = R_1$), (ii) space charge capacitance of the depletion layer ($Z_{sc} = (j\omega C_{sc})^{-1}$), where ω is the angular frequency, and (iii) electron−hole recombination, namely, charge diffusion ($Z_w = T_w^{-1}(j\omega)^{-0.5}$) and transport ($Z_2 = R_2$). Charge diffusion ($Z_w$) is modeled with the semi-infinite diffusion (Warburg) impedance, where the sample thickness is considerably larger than that of the depletion/space-charge layer. This component specifically accounts for the 45° slope of the low-frequency region (inset of Figure 5). The inclusion of the Z_2 resistance term was necessary given the poorer conductivity of hematite compared to that of the anatase used in the original circuit of Bondarenko and Ragoisha.[43] It may possibly account for processes including electron−hole recombination, charge diffusion and charge trapping in the conduction bands, and charge leakage due to structural defects and/or impurities. This term was also included in the recent study of Klahr et al.[6] on hematite photoelectrodes. Taking into account the serial and parallel combinations of these circuit elements, impedance contributions from the hematite bulk are expressed as follows:

$$Z_{hem} = \frac{1}{j\omega C_{sc} + \frac{1}{R_1 + \frac{1}{(j\omega)^{0.5}T_w + \frac{1}{R_2}}}} \quad (1)$$

Optimized values for each of these terms are reported in Table 1. These results readily suggest that charge diffusion in hematite is influenced more by the type of electrolyte ions present in the system rather than the solution pH itself. These differences are thereby attributed to interfacial interactions between the hematite surface and electrolyte ions.

Interfacial and solution processes become more significant at intermediate to low frequencies. These include contributions from (i) the capacitance of the diffuse layer ($Z_{dl} = (j\omega C_{dl})^{-1}$), (ii) the ionic adsorption capacitance ($Z_{CPE} = T_{ad}^{-1}(j\omega)^{-\varphi}$), here expressed in the form of a constant phase element (CPE), and (iii) adsorption resistance ($Z_{ad} = R_{ad}$). The capacitance (Z_{dl}) term of the diffuse layer arises from the response of free electrolyte ions. The terms of the compact plane pertain to the capacitive and resistive contributions of the transfer of potential-determining ions (H^+, OH^-) and ammonium species across the compact layer. The CPE was, in this case, required for the capacitance term to fit the data. The associated φ term was optimized to denote the nonideal behavior of the compact plane, which could be attributed to imperfections including a nonuniform current distribution and surface roughness. These circuit elements account for the remaining impedance, alongside the solution and other unknown instrument component resistances (R_s):

dx.doi.org/10.1021/la300829c | Langmuir 2012, 28, 7914−7920

Table 1. Output of the Equivalent Circuit Model for the Hematite Single-Crystal Electrode[a]

NaCl pH	χ^2 (10^{-5})	C_{dl} (μF·cm^{-2})	T_{ad} (μF·cm^{-2}·s$^{-\varphi}$)	φ	R_{ad} (kΩ·cm^2)	R_s (Ω·cm^2)	C_{sc} (nF·cm^{-2})	R_1 (kΩ·cm^2)	R_2 (kΩ·cm^2)	T_w (μF·cm^{-2}·s$^{-0.5}$)
3.8	5.86	2.50 (0.04)	33.03 (0.07)	0.72(0.001)	1.35 (0.01)	157.9 (1.2)	8.18 (0.07)	0.463 (0.007)	1.49 (0.01)	7.60 (0.15)
4.7	6.38	2.42 (0.04)	32.89 (0.07)	0.72 (0.001)	1.36 (0.01)	157.5 (1.3)	8.16 (0.07)	0.464 (0.007)	1.51 (0.01)	7.58 (0.16)
5.9	6.67	2.37 (0.04)	32.82 (0.07)	0.72 (0.001)	1.39 (0.01)	157.2 (1.3)	8.17 (0.07)	0.465 (0.007)	1.52 (0.01)	7.57 (0.16)
7.0	6.51	2.37 (0.04)	32.74 (0.07)	0.72 (0.001)	1.39 (0.01)	157.3 (1.3)	8.19 (0.07)	0.466 (0.007)	1.54 (0.01)	7.64 (0.16)
8.1	6.45	2.34 (0.04)	32.86 (0.07)	0.73 (0.001)	1.40 (0.01)	157.1 (1.3)	8.20 (0.07)	0.464 (0.007)	1.54 (0.01)	7.60 (0.16)
9.0	6.73	2.32 (0.04)	32.55 (0.07)	0.73 (0.001)	1.41 (0.01)	157.7 (1.3)	8.20 (0.07)	0.467 (0.007)	1.55 (0.01)	7.67 (0.16)
10.1	7.19	2.35 (0.04)	32.39 (0.07)	0.72 (0.001)	1.44 (0.01)	157.9 (1.4)	8.20 (0.07)	0.466 (0.007)	1.55 (0.01)	7.63 (0.16)
11.1	7.24	2.39 (0.04)	31.93 (0.07)	0.72 (0.001)	1.47 (0.01)	157.7 (1.4)	8.22 (0.07)	0.465 (0.007)	1.52 (0.01)	7.65 (0.17)
11.9	6.48	2.44 (0.04)	32.42 (0.07)	0.71 (0.001)	1.41 (0.01)	155.5 (1.3)	8.21 (0.07)	0.458 (0.007)	1.49 (0.01)	7.60 (0.16)
NH_4Cl pH	χ^2 (10^{-4})	C_{dl} (μF·cm^{-2})	T_{ad} (μF·cm^{-2}·s$^{-\varphi}$)	φ	R_{ad} (kΩ·cm^2)	R_s (Ω·cm^2)	C_{sc} (nF·cm^{-2})	R_1 (kΩ·cm^2)	R_2 (kΩ·cm^2)	T_w (μF·cm^{-2}·s$^{-0.5}$)
3.5	3.46	1.93 (0.10)	33.77 (0.16)	0.67 (0.002)	0.96 (0.03)	152.9 (3.1)	8.37 (0.18)	0.429 (0.016)	1.07 (0.02)	9.44 (0.62)
4.4	2.35	1.85 (0.08)	31.77 (0.12)	0.67 (0.002)	1.01 (0.02)	153.0 (2.5)	8.38 (0.15)	0.434 (0.013)	1.10 (0.02)	9.53 (0.51)
5.7	2.29	1.75 (0.08)	31.00 (0.12)	0.67 (0.002)	1.03 (0.02)	153.3 (2.5)	8.39 (0.14)	0.439 (0.013)	1.10 (0.02)	9.95 (0.52)
6.6	2.28	1.66 (0.08)	29.72 (0.11)	0.66 (0.002)	1.02 (0.02)	153.1 (2.5)	8.38 (0.15)	0.439 (0.013)	1.09 (0.02)	9.78 (0.53)
7.5	2.38	1.57 (0.08)	27.75 (0.11)	0.66 (0.002)	1.01 (0.03)	152.3 (2.6)	8.32 (0.15)	0.439 (0.014)	1.08 (0.02)	9.46 (0.55)
8.4	2.34	1.52 (0.07)	26.20 (0.10)	0.65 (0.002)	1.02 (0.03)	152.7 (2.6)	8.30 (0.15)	0.440 (0.015)	1.08 (0.02)	9.13 (0.55)
9.4	2.28	1.43 (0.07)	25.21 (0.10)	0.64 (0.002)	1.13 (0.03)	164.1 (2.6)	8.42 (0.15)	0.448 (0.015)	1.12 (0.03)	9.17 (0.54)
10.6	2.01	1.56 (0.09)	21.02 (0.07)	0.56 (0.002)	2.39 (0.11)	518.9 (3.1)	10.2 (0.15)	0.628 (0.012)	2.12 (0.13)	13.5 (0.52)

[a]Values are corrected for the geometrical surface area of the single-crystal electrode (0.222 cm^2). Standard deviations, errors, and confidence limits are given after multiplication by the Student t test results and are shown in parentheses.

$$Z = R_s + \frac{1}{j\omega C_{dl} + \frac{1}{R_{ad} + \frac{1}{(j\omega)^{\varphi} T_{ad}}}} \quad (2)$$

All optimal parameters are reported in Table 1. Parameters used in eqs 1 and 2 can reproduce all of the experimental data. Examples of the fit of the models to two of the data sets collected for this work are shown in Figure 5.

3.3.2. Equivalent Circuit Parameters. All C_{dl} values are in the 1.43−2.50 μF·cm^{-2} range, whereas the T_{ad} values are 1 order of magnitude greater, with values in the 21.02−33.03 μF·cm^{-2}·s$^{-\varphi}$ range with φ < 1 (Table 1). The greater capacitance of T_{ad} thereby denotes a thin molecular capacitor of relatively larger charge-storage capacity, such as that characteristic of compact layers. This capacitance, especially if it could be extracted in true units of μF·cm^{-2}, would have little effect on the overall capacitance of the interface. Therefore, because the C_{dl} values are comparable to those derived from C_{int} (section 3.1), in this respect cyclic voltammetry appears to provide an additional independent validation of the values derived by our circuit model.

The pH dependence of all compact and diffuse plane parameters is shown in Figure 6. In NaCl solutions, C_{dl} varies nonlinearly with pH from 2.32 to 2.50 μF·cm^{-2}, reaching a minimum at pH 9 (Figure 6a). Interestingly, this point is close to the point of zero charge (PZC) of colloidal hematite[44] and may possibly correspond to that of our imperfect electrode surface. If PZC = 9, then the contributions of all instrumental pH-insensitive potential differences of our electrochemical cell, E_{instr}, are 84 mV and the resulting $E_{OCP} - E_{instr}$ values become comparable to the range of values reported by Zarzycki et al.,[19] as are our aforementioned hysteresis-curve-derived E_{OCP} values obtained during preliminary sets of experiments. Values of C_{dl} for the NH_4Cl-bearing system (1.43−1.93 μF·cm^{-2}) are lower than in NaCl but also reach a minimum at pH 9. The lower values are attributed to coexisting ammonium ($\equiv Fe_xOH_y\cdots HNH_3$) and ammonia ($\equiv Fe_xOH_y\cdots NH_3$) surface species throughout the 2−12 pH range, with a pK_a of 8.3, are reported in a previous cryogenic XPS study of hematite colloids.[5]

T_{ad} values arise, in contrast to those of C_{dl}, from a CPE with φ values of 0.71−0.73 for NaCl and 0.56−0.67 for NH_4Cl. Values for NaCl are pH-independent and denote a constant capacitance of 32.57 ± 0.49 μF·cm^{-2}·s$^{-\varphi}$. Values for NH_4Cl-bearing systems, however, decrease from this value at pH 3.5 down to 21.0 μF·cm^{-2}·s$^{-\varphi}$ at pH 10.6. This dramatic decrease is ascribed to direct (hydrogen-bonded) interactions between ammonium species and surface (hydro)oxo groups,[5] which in turn alter the thickness of the compact layer. Likewise, the presence of ammonium species in the compact layer results in a decrease in interfacial resistance in relation to that of NaCl-bearing systems (Figure 6c).

Finally, it is noteworthy to mention that our surface-area-normalized capacitance values (Figure 6a,b) are about 1 order of magnitude smaller than those inferred by fitting the potentiometric titration data of iron oxide powders (e.g., 88 μF·cm^{-2} for Na^+ and 94 μF·cm^{-2} for NH_4^+).[45] This discrepancy, we believe, may arise from the thicker space-charge region of the electrode surface compared to that of the typical submicrometer-sized particles used in titration studies. We also note that EIS is a frequency-resolved method, separating slow chemical reactions from fast electrostatic reactions involving the transfer of ions through compact and diffuse layers. Titration studies, in contrast, derive capacitance values with thermodynamic models calibrated on analytical proton adsorption data.[46,47] These two notions of capacitance may therefore not be directly comparable. However, further work along such lines may help bridge the concepts of capacitance in the framework of EIS studies with respect to thermodynamic adsorption modeling.

dx.doi.org/10.1021/la300829c | Langmuir 2012, 28, 7914−7920

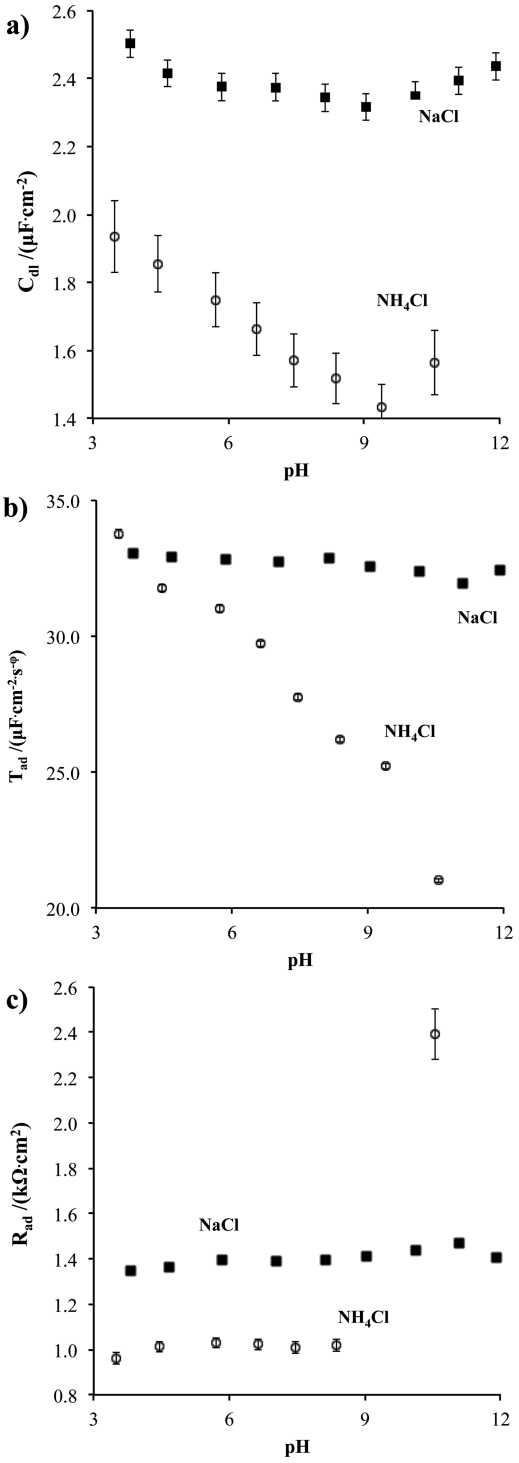

Figure 6. pH dependence of the capacitance and resistance components of the hematite/water interface: (a) diffuse layer capacitance (C_{dl}), (b) compact layer resistance (R_{ad}), and (c) CPE capacitance (T_{ad}). Note that the units of T_{ad} are $\mu F \cdot cm^{-2} \cdot s^{-\varphi}$ for $\varphi < 1$ because CPE is an imperfect capacitor. All results are corrected for the geometrical surface area of the electrode (0.222 cm^2).

4. CONCLUSIONS

We have demonstrated the use of EIS in measuring the interfacial properties of a single-body hematite working electrode. The method makes it possible to separate surface (de)protonation and the specific adsorption of electrolyte ions to investigate the dependency of the interfacial capacitance on the solution pH and the background electrolyte. Diffuse layer capacitances extracted by EIS lie in the 1.43−2.50 $\mu F/cm^2$ range and are affected by both the electrolyte type and pH. Those in the compact layer are 1 order of magnitude larger, with a value of 32.57 ± 0.57 $\mu F \cdot cm^{-2} \cdot s^{-\varphi}$ in NaCl. They are pH-independent in NaCl but are readily lowered by the hydrogen bonding of ammonia species with surface (hydr)oxo groups in NH_4Cl media, decreasing to 21.02 ± 0.3 $\mu F \cdot cm^{-2} \cdot s^{-\varphi}$ at high pH. The results obtained thus far suggest no significant transfer of Cl^- ions across the compact plane. Comparisons with different ionic strengths and media may help to assess this point further.

Given the promising outcomes of EIS studies of hematite/water interfaces, a number of additional investigations are currently underway. Forthcoming hematite EIS studies will notably involve the effects of sorbed ligands, etching and exposure to ultraviolet radiation using oriented surfaces of various crystallographic terminations. Such efforts, combined with other electrochemical,[19−24] interfacial structure,[9−16] microscopy,[17,18] and molecular modeling studies,[48−50] should thereby help further our understanding of physicochemical attributes of the hematite/water interface.

AUTHOR INFORMATION

Corresponding Author

*E-mail: jean-francois.boily@chem.umu.se. Tel: +46 90 786 5270.

Notes

The authors declare no competing financial interest.

ACKNOWLEDGMENTS

This work was supported by the Carl-Tyggers Foundation, the Swedish Research Council (2009-3110), and the Wallenberg Foundation.

REFERENCES

(1) Schwertmann, U.; Cornell, R. M. *The Iron Oxides*; Wiley-VCH: New York, 2003.
(2) Sivula, K.; Le Formal, F.; Grätzel, M. *ChemSusChem* **2011**, *4*, 432.
(3) Boily, J.-F.; Shchukarev, A. *J. Phys. Chem. C* **2010**, *114*, 2613−2616.
(4) Schudel, M.; Behrens, S. H.; Holthoff, H.; Kretzschmar, R.; Borkovec, M. *J. Colloid Interface Sci.* **1997**, *196*, 241−253.
(5) Shimizu, K.; Shchukarev., A.; Boily, J.-F. *J. Phys. Chem. C* **2011**, *115*, 6796−6801.
(6) Klahr, B.; Gimenez, S.; Fabregat-Santiago, F.; Hamann, T.; Bisquert, J. *J. Am .Chem. Soc.* **2012**, *134*, 4294−4302.
(7) Tilley, S. D.; Cornuz, M.; Sivula, K.; Grätzel, M. *Angew. Chem.* **2010**, 6405−6408.
(8) Yamamoto, S.; Kendelewicz, T.; Newberg, J. T.; Ketteler, G.; Starr, D. E.; Mysak, E. R.; Andersson, K. J.; Ogasawara, H.; Bluhm, H.; Salmeron, M.; Brown, G. E., Jr.; Nilsson, A. *J. Phys. Chem. C* **2010**, *114*, 2256−2266.
(9) Catalano, J. G.; Fenter, P.; Park, C. *Geochim. Cosmochim. Acta* **2007**, *71*, 5313−5324.
(10) Catalano, J. G.; Fenter, P.; Park, C. *Geochim. Cosmochim. Acta* **2009**, *73*, 2242−2251.
(11) Catalano, J. G. *Geochim. Cosmochim. Acta* **2011**, *75*, 2062−2071.
(12) Tanwar, K. S.; Catalano, J. G.; Petitto, S. C.; Ghose, S. K.; Eng, P. J.; Trainor, T. P. *Surf. Sci.* **2007**, *601*, L59−L64.
(13) Tanwar, K. S.; Lo, C. S.; Eng, P. J.; Catalano, J. G.; Walko, D. A.; Brown, G. E., Jr.; Waychunas, G. A.; Chaka, A. M.; Trainor, T. P. *Surf. Sci.* **2007**, *601*, 460−474.
(14) Tanwar, K. S.; Petitto, S. C.; Ghose, S. K.; Eng, P. J.; Trainor, T. P. *Geochim. Cosmochim. Acta* **2008**, *72*, 3311−3325.

(15) Tanwar, K. S.; Petitto, S. C.; Ghose, S. K.; Eng, P. J.; Trainor, T. P. *Geochim. Cosmochim. Acta* **2009**, *73*, 4346−4365.
(16) Catalano, J. G.; Zhang, Z.; Park, C.; Fenter, P.; Bedzyk, M. J. *Geochim. Cosmochim. Acta* **2007**, *71*, 1883−1897.
(17) Eggleston, C. M. *Am. Mineral.* **1999**, *84*, 1061−1070.
(18) Eggleston, C. M.; Stack, A. G.; Rosso, K. M.; Higgins, S. R.; Bice, A. M.; Boese, S. W.; Pribyl, R. D.; Nichols, J. J. *Geochim. Cosmochim. Acta* **2003**, *67*, 985−1000.
(19) Zarzycki., P.; Chatman, S.; Preočanin, T.; Rosso, K. M. *Langmuir* **2011**, *13*, 7986−7990.
(20) Yanina, S. V.; Rosso, K. M. *Science* **2008**, *320*, 218−222.
(21) Boily, J.-F.; Chatman, S.; Rosso, K. M. *Geochim. Cosmochim. Acta 727* **2011**, *75*, 4113−4124.
(22) Eggleston, C. M.; Shankle, A. J. A.; Moyer, A. J.; Cesar, I.; Grätzel, M. *Aquat. Sci.* **2009**, *71*, 151−159.
(23) Kallay, N.; Preočanin, T. J. *Colloid Interface Sci.* **2008**, *318*, 290−295.
(24) Preočanin, T.; Čop, A.; Kallay, N. J. *Colloid Interface Sci.* **2006**, *299*, 772−776.
(25) Lopes, T.; Andrade, L.; Aguilar Ribeiro, H.; Mendes, A. *Int. J. Hydrogen Energy* **2010**, *35*, 11601−11608.
(26) BAk, Y.; Choi, W.; Park, H. *Appl. Catal. B* **2011**, *110*, 207−215.
(27) Mulmudi, H. K.; Mathews, N.; Dou, X. C.; Xi, L. F.; Pramana, S. S.; Lam, Y.M-; Mhaisalkar, S. G. *Electrochem. Commun.* **2011**, *13*, 951−954.
(28) Karthik, K. R. G.; Mulmudi, H. K.; Jinesh, K. B.; Matthews, N.; Sow, C. H.; Huang, Y. Z.; Mhaisalkar, S. G. *Appl. Phys. Lett.* **2011**, *99*, 132105.
(29) Strmcnik, D.; van der Vliet, D. F.; Chang, K.-C.; Komanicky, V.; Kodama, K.; You, H.; Stamenkovic, V. R.; Marković, N. M. *J. Phys. Chem. Lett.* **2011**, *2*, 2733−2736.
(30) Gabrielli, C.; Grand, P. P.; Lasia, A.; Perrot, H. *J. Electrochem. Soc.* **2004**, *151*, A1943−A1949.
(31) Hens, Z.; Gomes, W. P. *Phys. Chem. Chem. Phys.* **1999**, *1*, 3607−3615.
(32) Shimizu, K.; Shchukarev, A.; Kozin, Ph.; Boily, J.-F. *Surf. Sci.* **2012**, in press.
(33) Boukamp, B. A. *Solid State Ionics* **2004**, *169*, 65−73.
(34) Boukamp, B. A. *J. Electrochem. Soc.* **1995**, *142*, 1885−1894.
(35) Mulvaney, P.; Cooper, R.; Grieser, F.; Meisel, D. *Langmuir* **1988**, *4*, 1206−1211.
(36) Jang, K. H.; Dempsey, B. A.; Burgos, W. D. *Environ. Sci. Technol.* **2007**, *41*, 7303−7308.
(37) Cummings, C. Y.; Bonné, M. J.; Edler, K. J.; Helton, M.; McKee, A.; Marken, F. *Electrochem. Commun.* **2008**, *10*, 1773−1776.
(38) Bora, D. K.; Braun, A.; Erat, S.; Ariffin, A. K.; Löhnert, R; Sivula, K.; Töpfer, J.; Grätzel, M.; Manzke, R.; Graule, T.; Constable, E. C. *J. Phys. Chem. C* **2011**, *115*, 5619−5625.
(39) Wijayantha, U. K. G.; Saremi-Yarahmadi, S.; Peter, L. M. *Phys. Chem. Chem. Phys.* **2011**, *13*, 5264−5270.
(40) Yu, X.; Licht, S. *J. Power Sources* **2007**, *171*, 966−980.
(41) Bouzek, K.; Roušar, I. *J. Appl. Electrochem.* **1996**, *26*, 919−923.
(42) Bard, A. J.; Faulkner, L. R. *Electrochemical Methods*, 2nd ed.; John Wiley & Sons: New York, 2000.
(43) Bondarenko, A. S.; Ragoisha, G. A. *J. Solid State Electrochem.* **2005**, *9*, 845−849.
(44) Breeuwsma, A.; Lyklema, J. *J. Colloid Interface Sci.* **1973**, *43*, 437−448.
(45) Sverjensky, D. A. *Geochim. Cosmochim. Acta* **2005**, *69*, 225−257.
(46) Boily, J.-F.; Lützenkirchen, J.; Balmès, O.; Beattie, J.; Sjöberg, S. *Colloids Surf., A* **2001**, *179*, 11−27.
(47) Hiemstra, T.; van Riemsdijk, W. H. *J. Colloid Interface Sci.* **2006**, *301*, 1−18.
(48) Kerisit, S. *Geochim. Cosmochim. Acta* **2011**, *75*, 2043−2061.
(49) Rustad, J. R.; Wasserman, E.; Felmy, A. R. *Surf. Sci.* **1999**, *424*, 28−35.
(50) Yin, S.; Ellis, D. E. *Surf. Sic.* **2008**, *602*, 2047−2054.